Ultrashort electron bunches with subfemtosecond jitter from an *X*-band photocathode rf gun

Zixin Guo, Biaobin Li, Cheng Li, Haoran Zhang, Xiazhen Xu, Jingya Li, Zhigang He,* Shancai Zhang, and Lin Wang

National Synchrotron Radiation Laboratory, University of Science and Technology of China, Hefei, Anhui 230029, China

(Received 21 March 2023; accepted 20 November 2023; published 12 December 2023)

The ultrafast electron beam diffraction technology, which involves an electron beam at the level of several megaelectron volts, is crucial for studying ultrafast dynamic processes at the atomic level. To discern these processes at a temporal resolution of a few femtoseconds, the demand to focus on electron beams with femtosecond or even subfemtosecond width and time jitter is increasing. In this paper, we investigate the dynamics of electron beams as they interact with lasers, present an explanation of the mechanism that results in time jitter, and propose a method to mitigate or possibly eliminate the time jitter by inducing a specific energy chirp in the electron beam through the use of *X*-band photocathode rf gun. The feasibility of this method is confirmed by implementing bunch compression with two radially polarized laser pulses. Simulation results demonstrate that the time jitter can be reduced to less than 1 fs when the amplitude jitter of the rf gun is within $\pm 0.05\%$ and the phase jitter is within $\pm 0.5°$. Based on our findings, we anticipate that this approach will substantially advance the field of ultrafast science and technology.

DOI: 10.1103/PhysRevAccelBeams.26.123401

I. INTRODUCTION

Ultrafast electron diffraction (UED) is a powerful research tool that enables the study of atomic-level ultrafast dynamic processes [1–8]. To improve its time resolution, it is crucial to reduce the electron beam's pulse width and flight-time jitter.

UED facilities utilize the photocathode laser to drive the photocathode of the electron gun, thereby generating photoelectrons that are subsequently accelerated and applied to measure the sample structure. To achieve a single-shot diffraction spot measurement, the electron bunch must contain at least 10^4–10^5 electrons [9]. However, it is difficult to collect so many electrons within an ultrashort pulse due to the existence of the space charge repulsion force. To overcome this problem, a UED scheme utilizing a relativistic electron beam with the energy of several megaelectron volts (MeV-UED) has been proposed [10] based on the physical property that pulse broadening caused by space charge force is proportional to $1/\gamma^2$ (γ is the Lorentz factor). To rapidly accelerate the beam to relativistic speed, an rf gun cavity, with an acceleration gradient up to 100 MV/m level, is employed. Although the response time of a metal photocathode (such as copper) is predicted to be less than 1 fs, the width of the electron pulse emitted from the cathode is broader than that of the driving laser pulse due to the thermal emittance of the electron beam [11]. The difference in angles of electrons leaving the cathode leads to different velocities along the beam moving direction, causing the broadening of the pulse. Additionally, the space charge repulsion force results in further pulse broadening, mainly before the beam is accelerated to the relativistic speed. In summary, no matter how short the driving laser pulse is, the order of electron pulse width emitted from the electron gun is around 100 fs. To further reduce the pulse width, various bunch compression techniques have been proposed and demonstrated [9,12–27]. One classical method involves introducing a microwave bunching cavity downstream of the photocathode rf gun [9,15,16]. The electron beam interacts with the microwave electric field, causing the electrons at the tail of the beam to move faster than those at the head. Then the pulse width can be minimized after passing through a drift section of a certain length. Using this method, the pulse width can be compressed to several fs [15,16]. However, in addition to pulse width, the time jitter of the electron beam serves as another major factor limiting the time resolution. In an rf gun, the accelerating electric field can be approximated as $E_0 \sin \phi$, where E_0 signifies the electric field amplitude, and ϕ denotes the phase. Fluctuations in its amplitude and phase will cause

*hezhg@ustc.edu.cn

variations in the electron beam energy, leading to flight time fluctuations from the cathode to the sample. Moreover, the use of an additional bunching cavity introduces another error source that exacerbates flight time jitter. In order to further reduce the flight time jitter, a double-bend achromatic magnetic compression technique has been proposed. It can not only compress the pulse width but also restrain the flight time jitter and make the time resolution of MeV-UED breaks through 50 fs [18], while the pulse width is 29 fs (FWHM) [18] and the time jitter is less than 7.8 fs [19].

Further improvement of temporal resolution will provide numerous opportunities for the field of ultrafast science. Pushing the temporal resolution to less than 10 fs will permit the exploration of electrically driven dynamics and high-frequency optical phonon modes [1]. Improving the temporal resolution to 1–2 fs allows for the precise observance of the dynamics of charge transfer in pure nuclear wave packets and molecules [28,29].

Recently, a novel approach utilizing radially polarized lasers has been developed to compress electron beams to sub-fs pulse width and achieve a time jitter of 1.35 fs [27]. However, achieving such a time jitter requires an amplitude accuracy of 0.0065% and a phase accuracy of 0.02°, which poses significant accuracy challenges to the rf gun.

This paper analyzes the dynamics of ultrashort electron beam production through laser-electron interaction, explains the mechanism of time jitter, and proposes a novel method to mitigate or possibly eliminate it. By exploiting the linear energy chirp of the electron beam, the compressed beam's central energy can be maintained constant, irrespective of the electron beam's average energy variation. As a result, it ensures that the time taken for the electron beam to travel to the sample after interaction remains unchanged. To validate the feasibility of this method, we consider the bunch compression scheme discussed in Ref. [27] as an illustrative example. Simulation results demonstrate that the time jitter can be restricted to less than 1 fs when the electric field amplitude jitter of the rf gun is within ±0.05% and the phase jitter is within ±0.5°.

II. MECHANISM OF TIME JITTER

The use of laser-electron interaction is a crucial method of generating ultrashort electron beams. Several bunch compression methods, such as using ponderomotive force potential [14], terahertz laser pulses [22,23], and radially polarized laser [27], have been proposed and validated. The fundamental principle behind these methods is to manipulate the laser pulse to generate a quasisinusoidal longitudinal photoelectric field with a period interval greater than the length of the electron beam. Then this field is utilized to modulate the electron beam, effectively reversing its longitudinal phase space. The physical image of the interaction between electron beam and laser can be summarized as shown in Fig. 1.

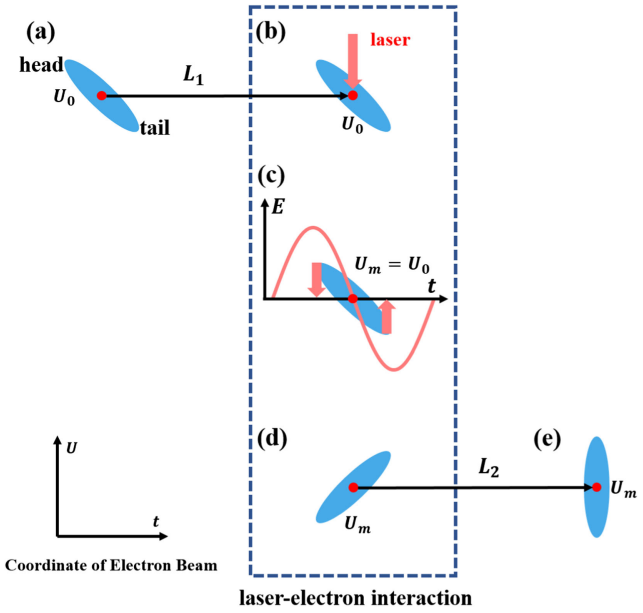

FIG. 1. The longitudinal phase space evolution of the ultrashort electron beam generated by laser-electron interaction. The coordinate system in the lower left-hand corner represents the longitudinal phase space of the electron beam, where the horizontal axis represents time t and the vertical axis represents energy U. (a) represents the electron beam at the gun exit, (b) indicates that the electron beam and laser arrive simultaneously at the modulation point, (c) illustrates the interaction between the electron beam and the laser, (d) demonstrates the electron beam after modulation, and (e) is the bunched electron beam at the sample.

Assuming an electron beam with an average energy of U_0 and a positive linear energy chirp is released from the electron gun exit as shown in Fig. 1(a). After traversing a drift section L_1, the beam reaches the modulation point in synchronization with a laser pulse [Fig. 1(b)] that has a quasisinusoidal longitudinal photoelectric field [the red curve in Fig. 1(c)]. When the laser and electron beam interact [Fig. 1(c)], the zero-intensity point of the photoelectric field aligns with a specific longitudinal position of the electron beam, where the corresponding energy of electrons is denoted as U_m. In order to achieve a symmetrical compression of the electron beam, U_m is usually set as U_0, which is at the longitudinal center of the electron beam. Compared to electrons at the position where the energy is U_m, electrons located at the head or tail of the electron beam, experience an electric field of different directions, resulting in a corresponding loss or gain of energy. Consequently, the electrons at the tail have higher energy than those at the head, causing a reversal of the longitudinal phase space [Fig. 1(d)]. To convert energy modulation to density modulation, a drift section L_2 follows. From a spatial perspective, this process is observed as electrons on both sides of the electron beam gradually converging toward the position occupied by electrons with energy

U_m, ultimately forming a high intense ultrashort electron pulse at the sample [Fig. 1(e)]. Thus, energy U_m actually represents the central energy of the compressed electron beam.

Once the energy of the laser pulse is specified, the energy difference between the head and tail of the modulated electron beam is constant. As a result, the length of the drift section L_2 is fixed. Therefore, the time required for the electron beam to pass through the drift section L_2 can be expressed as $t_s = L_2/v_m$, where v_m represents the velocity of electrons with energy U_m.

In the ideal case without jitter, U_m is equivalent to U_0. In reality, however, amplitude and phase jitter in the photocathode rf gun result in a change in the average energy of the electron beam. This, in turn, impacts the time it takes for the electron beam to traverse L_1 and reach the modulation point. The laser pulse is assumed to arrive at the modulation point in synchronization with the electron beam, which has an average energy of U_0. Due to the difference in arrival time, there is a shift in the longitudinal position of the electron beam that aligns with the zero-intensity point of the laser pulse. As a consequence, this shift leads to a change in the energy U_m. Thus, the time (t_s) of the electron beam passing drift section L_2 alters, which generates time jitter.

III. PRINCIPLE OF TIME JITTER MITIGATE

As discussed in Sec. II, minimizing the jitter in flight time of the compressed electron beam requires maintaining U_m as constant as possible. One widely accepted and commonly employed method to achieve this goal is to enhance the amplitude and phase stability of the rf gun, thus ensuring consistency in the output energy of the electron beam. One benefit of this method is that it reduces the variation in the time that the electron beam reaches the modulation point and, thereby, minimizes changes in U_m. However, this method presents great challenges to engineering technology and is difficult to maintain in the long term.

Instead of focusing on maintaining the stability of the electron gun's output energy, it is more advisable to directly preserve U_m. Since the laser operates in synchronization with the electron beam whose average energy is U_0, the time of the laser's arrival at the modulation point can be represented as $t_{\text{laser}} = L_1/v_0$ where v_0 is the velocity of electrons with energy U_0. In the case of a higher average energy of the electron beam, U_1, and average velocity, v_1, the longitudinal center of the electron beam will pass through a distance of $L_1' = v_1 t_{\text{laser}}$ upon the laser's arrival. This distance is greater than L_1 and causes the tail electrons, which are positioned at $d = L_1' - L_1$ away from the center position of the electron beam, to align with the laser pulse's zero-intensity point. If we want to make U_m equal to U_0, the electron beam must have a linear energy chirp, h, so that the energy U_m can be expressed as $U_m = U_1 - dh$. Then the chirp h can be deduced as Eq. (1).

$$h = \frac{U_1 - U_0}{d} = \frac{U_1 - U_0}{L_1(v_1/v_0 - 1)}. \tag{1}$$

By rearranging Eq. (1) and substituting the velocity v with the energy U, through their conversion relationship, Eq. (1) can be rewritten as Eq. (2) based on the fitting result of the calculated data from Eq. (1). It can be concluded that the required chirp h is inversely proportional to the distance L_1 and tends to increase as the average energy U_0 of the ideal electron beam increases.

$$h = \frac{U_0}{L_1}\frac{\left(\frac{U_1}{U_0} - 1\right)}{\left(\frac{v_1}{v_0} - 1\right)} \approx \frac{U_0}{L_1}(3.82U_0^2 - 0.99). \tag{2}$$

When the energy chirp h is achieved by appropriately adjusting both the average energy U_0 and the length of the drift section L_1, the longitudinal phase space of the electron beam at the modulation point and current intensity distribution of the compressed beam at the sample are demonstrated in Fig. 2. For an ideal case with no jitter, as shown in Fig. 2(b), the electron beam's center coincides with the zero-intensity point of the laser pulse, leading to a symmetric compression of the electron beam into an ultrashort pulse. Specifically, Figs. 2(a) and 2(c) demonstrate that the zero-intensity point

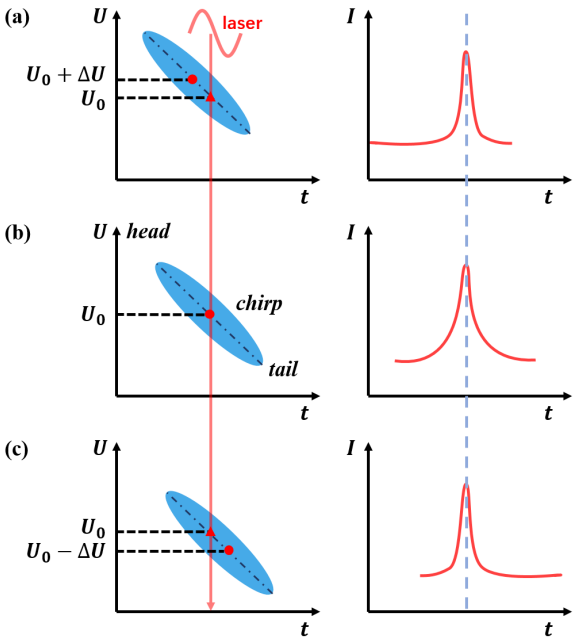

FIG. 2. Illustration of the employed jitter mitigation scheme. The left column represents the longitudinal phase space of the electron beam at the modulation point, and the right column represents the electron beam intensity distribution at the sample. (a), (b), and (c) for the cases where the average energy of the electron beam is greater than, equal to, and less than U_0, respectively.

of the laser pulse coincides with electrons having an energy of U_0 regardless of any fluctuations in the average energy of the electron beam, leading to the same arrival time from the modulation point to the sample. However, since the laser pulses no longer modulate the longitudinal center of the electron beam, the corresponding current intensity distribution is asymmetric.

It should be noted that Eq. (1) is derived based on the linear relationship between the flight time and the average energy of the electron beam within the drift section L_1. To extend the applicability of Eq. (1) to the entire process from the photocathode to the modulation point, it is essential to ensure that this linear relationship holds within the electron gun as well. In the gun rf cavity, electrons are emitted from the photocathode surface at low velocities and must undergo a phase slip process, as the velocity of the electron beam at the early acceleration stage is lower than that of the rf phase. Although the average energy difference of the electron beam exiting the gun may be small across different rf injection phases, the beam's flight time within the gun might differ considerably. To address the injection phase's influence on the linear relationship between flight time and average energy within the gun, we take advantage of a 2.3-cell structure (0.4:0.9:1) photocathode rf gun [18], allowing the electron beam to attain the highest energy and shortest flight time simultaneously for a specific injection phase.

IV. SIMULATION VERIFICATION

In this section, we employ General Particle Tracer [30], a particle motion simulation software, to conduct some simulations and validate the jitter mitigation method proposed in Sec. III.

To meet the required energy chirp of the electron beam, we design a 2.3-cell photocathode gun operating in the *X*-band (11.424 GHz). This design is based on a comprehensive assessment of several factors, including the electron beam average energy U_0, energy chirp h, drift section length L_1, and bunch compression.

According to Eq. (1), it can be estimated that the required chirp for an electron beam with energy in the range of several megaelectron volts is around 100–200 MeV/m. For the S-band (2856 MHz) rf field used in previous UED studies [9,16,18–20,22–24,26,27,31], the corresponding energy chirp is few tens of MeV/m, which is less than the required chirp. Although the requirements for the chirp can be relaxed by decreasing the energy U_0 and extending the distance L_1, the impact of the space charge force on bunch compression will be more significant. Considering this factor, we decide to maintain the electron beam's energy in the range of several megaelectron volts.

The energy chirp is determined by the rf gun field and the space charge force, with the rf field acting as the dominant factor. Specifically, the energy chirp originating from the rf field is proportional to the phase range of the electron beam's pulse width. Since the frequency of the *X*-band (11.424 GHz) microwave is 4 times that of the S-band (2856 MHz), the same bunch length occupies a phase range 4 times longer. Thus, using an *X*-band photocathode rf gun, we can generate an energy chirp that meets the requirement and effectively reduces time jitter. We design such a 2.3-cell *X*-band electron rf gun cavity and present the relevant dynamic curves inside the gun in Fig. 3. When the electric field's amplitude E_0 inside the gun is 190 MV/m (as is achievable according to previous studies [32–36]), we attain the optimum injection phase at 334.5°, resulting in a corresponding electron beam energy of 3.029 MeV.

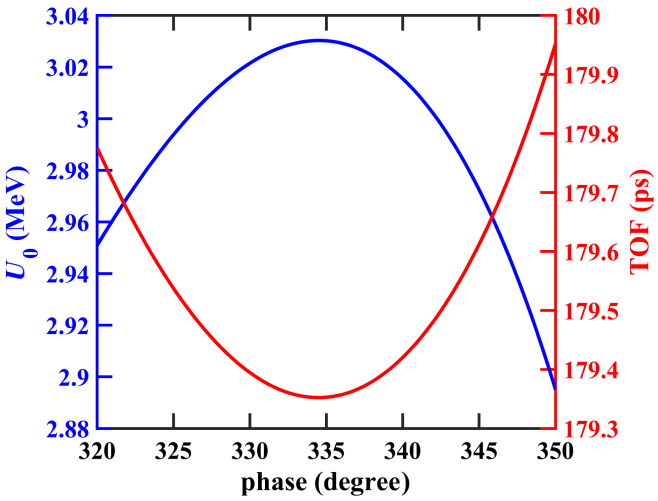

FIG. 3. The relationship between the beam energy, the time of flight in the gun, and the injection phase.

An electron beam with a charge of 10 fC is produced by irradiating a photocathode laser that measures 50 fs in length and has a radius of 50 μm on the surface of the photocathode. Further simulations are conducted by adopting the bunch compression method utilized in Ref. [27] as a model. The schematic layout is shown in Fig. 4 and the primary simulation parameters are detailed in Table I.

For a drift section length L_1 of 0.635 m, the electron beam is focused by the Solenoid 1 and has a radius of 3 μm at the modulation point. The longitudinal phase space of the electron beam at the modulation point is depicted in Figs. 5(a) and 5(b), with and without space charge force, respectively. Thanks to the space charge force, the energy difference between electrons at head and tail of the beam is further amplified, and the linearity of energy chirp is also improved. As a result, an energy chirp of 176.5 MeV/m, which meets the requirement, is achieved. This energy chirp is higher than that of the S-band rf gun, thus requiring a higher laser energy to invert the longitudinal phase space for achieving bunch compression.

Subsequently, the electron beam interacts with two radially polarized lasers with different wavelengths of 800 nm and 810.8 nm. The expression of radially polarized laser field can be found in Ref. [37]. The frequency difference between

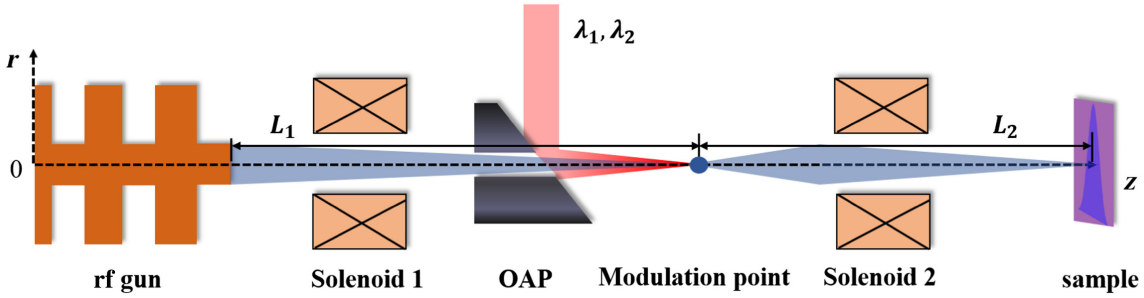

FIG. 4. The schematic layout.

the two laser pulses results in the formation of a quasisinusoidal photoelectric field with a period of 200 fs, as shown in the equation $T = 2\pi/(\omega_1 - \omega_2)$. Here, ω_1 and ω_2 are the angular frequencies of the lasers with central wavelengths λ_1 and λ_2, respectively. The period is longer than the electron beam length of 100 fs. In order to enhance the intensity of the photoelectric field, the two radially polarized pulses' transverse size is focused to 5 μm using an off-axis parabolic mirror. Each beam has a pulse width of 0.2 ps, and the peak photoelectric field is 7.5×10^{11} V/m when the energy of a single beam laser is 3.2 mJ.

After achieving energy modulation, as shown in Fig. 6, the electron beam then undergoes a drift section L_2, which is 0.24 m, to form density modulation. The blue curve in Fig. 7 displays the formed high current intensity spike, with an FWHM of 7.72 fs, and a total pulse width of 14.92 fs (rms). In UED experiments, each electron in the beam contributes equally to the signal detected on the screen. Therefore, the actual temporal resolution for sampling ultrafast dynamical signals is not simply dominated by the 7.72-fs current spike. For different types of ultrafast dynamical signals, such as a non-Gaussian and complex

TABLE I. Main parameters.

Parameters	Values
Parameters of the gun	
Electric field amplitude E_0	190 MV/m
Frequency	11.424 GHz
Launch phase ϕ	334.5°
Initial electron beam parameters	
Beam charge	10 fC
Number of electrons	62 415
Radius (uniform)	50 μm
Initial pulse duration (uniform)	50 fs
Thermal emittance (normalized)	12.7 nm rad
Solenoid 1 parameters	
Solenoid strength	0.20 T
The effective length	0.15 m
Solenoid 2 parameters	
Solenoid strength	0.31 T
The effective length	0.15 m
Two-color RPL pulse parameters	
Pulse duration (Gaussian, FWHM)	0.2 ps
Radius at the focus location	5 μm
Central wavelength	800 nm/810.8 nm
Pulse energy	3.2 mJ

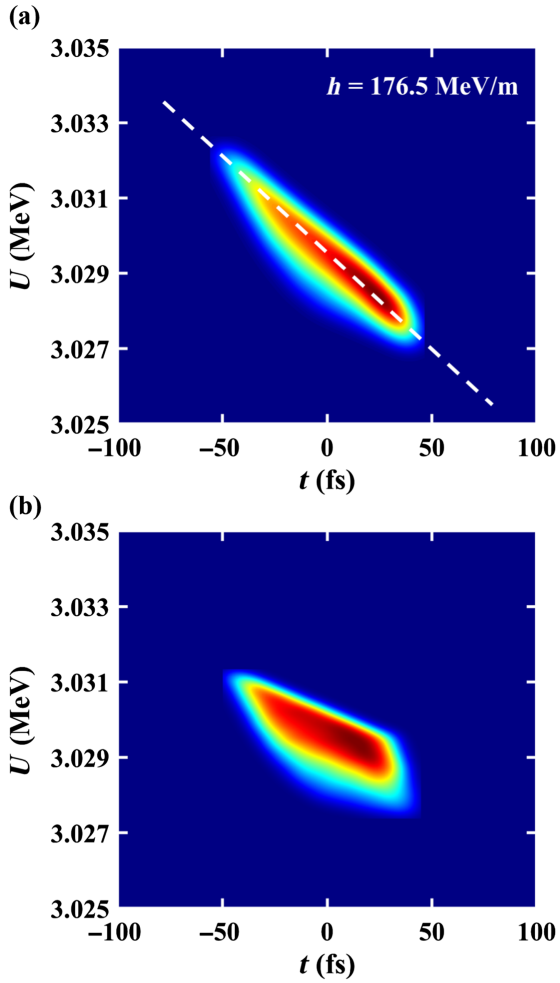

FIG. 5. Longitudinal phase space of electron beam at the modulation point. The head of the electron beam is on the left and the tail is on the right. (a) With the space charge force, the chirp is 176.5 MeV/m; (b) without the space charge force, the chirp is 147.7 MeV/m.

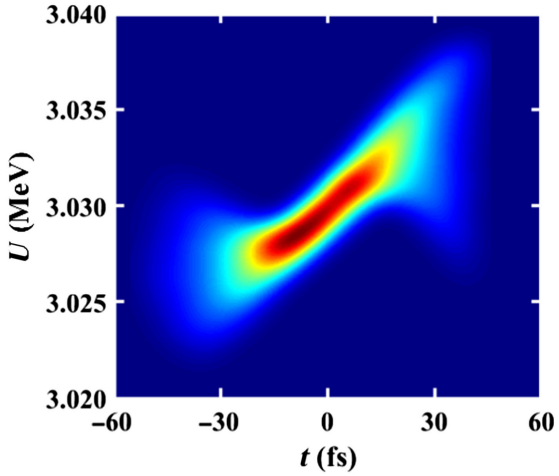

FIG. 6. Longitudinal phase space of electron beam after the modulation. The head of the electron beam is on the left and the tail is on the right.

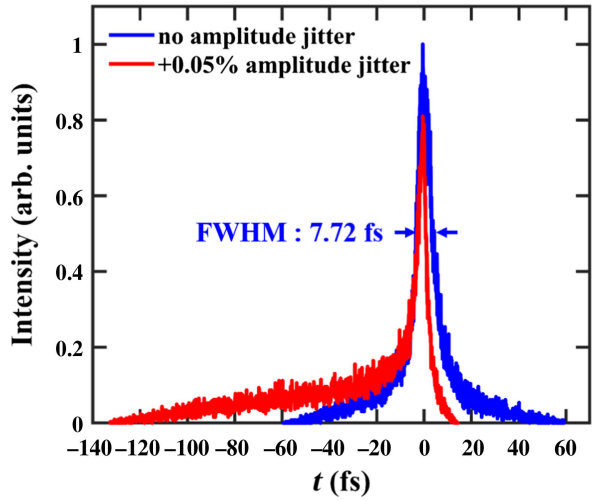

FIG. 7. The compressed electron beam at the sample, without amplitude jitter of the rf gun (blue), and with a positive 0.05% amplitude jitter (red).

current distribution will have different temporal resolutions, as discussed in Ref. [38].

At the sample position, the beam's transverse size is focused to 1.3 μm (rms) by the solenoid 2, and the normalized emittance is 17.28 nm rad. The laser pulses arrive at the sample position 9.02 ps ahead of the electron beam, displaying a hollow ring-shaped intensity distribution, and the radius of the hollow spot is approximately 2 mm. Since the electron beam has an rms radius of 1.3 μm at the sample position, the residual laser energy will not interfere with the UED experiment.

The next step is to analyze the effect of the rf gun's amplitude E_0 and phase ϕ fluctuation on the time jitter of the compressed electron beam. The simulation result illustrated in Fig. 8 shows that time jitter can be confined

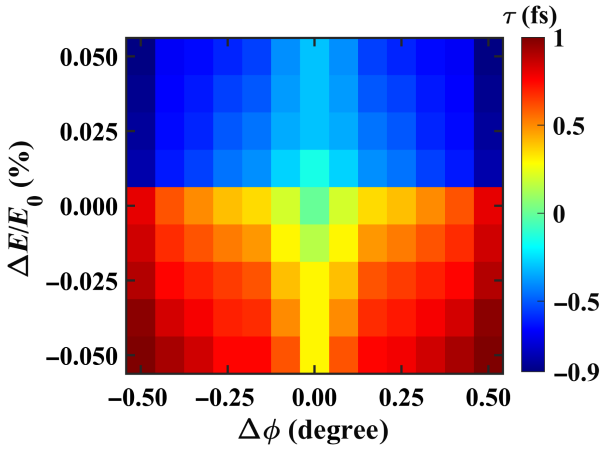

FIG. 8. The time jitter τ of the compressed electron beam arriving at the sample position caused by the phase and amplitude jitter.

to less than 1 fs when the amplitude jitter of the rf gun remains within ±0.05% and the phase jitter remains within ±0.5°. Compared to the previous simulation results [27], where a time jitter below 1.35 fs is obtained within an amplitude accuracy of 0.0065% and a phase accuracy of 0.02°, this jitter mitigation method further enables the electron beam to achieve sub-fs time jitter. Moreover, it enhances the beam's tolerance toward the amplitude and phase jitter of the rf gun, which has increased by 1 order of magnitude, making the method achievable with current technology. As reported in Ref. [33], measurements show that the shot-to-shot amplitude jitter of the *X*-band rf gun can be 0.01% and the phase stability can be maintained below 0.5°. It is also worth noting that the emittance of the compressed electron beam at the sample position will not be affected by amplitude and phase jitter within the given range.

In Fig. 8, the maximum amplitude jitter is set as ±0.05%. When the amplitude jitter reaches 0.05%, the tail part of the electron beam undergoes modulation by the laser, resulting in an asymmetric distribution of the compressed beam, as the red curve shown in Fig. 7. If the amplitude deviation exceeds this value, the electron beam will miss the modulation laser. One possible approach to address this issue is to increase the initial beam's bunch length. It is also worth noting that the proposed scheme can tolerate a larger phase fluctuation. According to simulation results, a 1° phase fluctuation leads to a time jitter of 2.4 fs.

Figure 8 also demonstrates that the time jitter performance is slightly better for a positive amplitude deviation compared to a negative one. This phenomenon can be explained as follows. In Fig. 3, the ideal injection phase corresponds to the minimum flight time. If there is any phase fluctuation, the electron beam's flight time in the gun is increased, and it reaches the laser modulation point later in time. However, a positive amplitude deviation gives the

electron beam higher energy, shortening the time from the gun exit to the modulation point. Consequently, the electron's energy at the central modulation position is closer to U_0.

V. DISCUSSION

Section IV analyzes the impact of amplitude and phase fluctuations of the rf gun on the flight time jitter under the assumption of perfect laser synchronization. In the following, we will discuss how the jitter in the modulation laser affects the flight time jitter of the compressed bunch, assuming no fluctuations in the rf gun and a constant average energy of U_0 for the electron beam.

A time delay t_{pl} between the photocathode laser and the modulation laser will lead to a shift in the longitudinal position of the electron beam corresponding to the laser's zero-intensity point, thereby changing the central energy U_0 of the compressed electron beam. The energy variation can be expressed as $\Delta U = ht_{pl}c$, where c represents the speed of light. In particular, a time jitter of 1 fs between the photocathode laser and the modulation laser will result in a flight time jitter of 0.5 fs. In pump-probe experiments, the presence of the pump laser will introduce another time jitter.

Furthermore, the assumption of a constant 180° phase difference between the two modulation laser pulses at the modulation point may be disrupted by factors like group velocity dispersion and environmental temperature, which impact laser propagation. These factors can also cause an offset in the zero-intensity point of the formed photoelectric field and a variation in the corresponding electron energy. For instance, a phase jitter of 1° will cause a flight time jitter of 0.25 fs.

Taking into account all the aforementioned factors, the flight time jitter of the electron beam can be statistically quantified using the root mean square of all time jitters.

In practical applications, a seed-oscillated laser can be employed to drive two amplifiers, generating lasers with different central wavelengths. These lasers are then utilized to generate the photocathode and pump laser using either the harmonic generator or optical parametric amplifier. Since all the lasers originate from the same source, there is an effective mitigation of the time jitter between them and their carrier phase remains stable. Additionally, both modulation lasers share the same propagation path, thereby ensuring that they are subject to the same environment.

The applicability of this scheme is also worth discussing. Although the compression of electron beams with dual-wavelength radially polarized lasers is used as an example, this jitter mitigation method can be extended to other compression methods based on laser-electron interactions, such as ponderomotive force potential bunch compression [14] and THz-driven bunch compression [22–24].

To successfully apply it in UED with energies of several megaelectron volts, there are still three critical factors that need consideration. First, the dark current problem needs to be considered, given the higher required acceleration gradient in comparison to the S-band gun. Second, studying methods for improving the gun's repetition rate while considering the heating problem is necessary. Finally, careful evaluation of the machining tolerance of the rf cavity is essential to ensure achieving the highest electron beam energy and the lowest flight time in the gun with the same injection phase.

VI. CONCLUSION

This paper proposes a new jitter mitigation method that can be applied to all bunch compression schemes based on laser-electron interaction. By generating an electron beam with a specific energy chirp using a 2.3-cell X-band rf gun, the energy on the electron beam's longitudinal position corresponding to the zero-intensity point of the quasisinusoidal longitudinal optical field remains constant, regardless of the average energy of the electron beam. This method effectively mitigates the time jitter of the compressed electron beam and reduces the accuracy requirements for the rf gun. The verification of this method is carried out through a bunch compression scheme based on dual-wavelength radially polarized laser pulses, and the simulation result shows that an initial beam length of 100 fs and 10 fC charge can be compressed to 7.72 fs (FWHM). The time jitter can also be confined to less than 1 fs when there is a amplitude jitter within $\pm 0.05\%$ and a phase jitter within $\pm 0.5°$.

ACKNOWLEDGMENTS

This work is supported by the Youth Innovation Promotion Association (CAS).

[1] D. Filippetto, P. Musumeci, R. Li, B. J. Siwick, M. Otto, M. Centurion, and J. Nunes, Ultrafast electron diffraction: Visualizing dynamic states of matter, Rev. Mod. Phys. **94**, 045004 (2022).

[2] M.-F. Lin, N. Singh, S. Liang, M. Mo, J. Nunes, K. Ledbetter, J. Yang, M. Kozina, S. Weathersby, X. Shen *et al.*, Imaging the short-lived hydroxyl-hydronium pair in ionized liquid water, Science **374**, 92 (2021).

[3] A. Sood, X. Shen, Y. Shi, S. Kumar, S. J. Park, M. Zajac, Y. Sun, L.-Q. Chen, S. Ramanathan, X. Wang *et al.*, Universal phase dynamics in VO_2 switches revealed by ultrafast operando diffraction, Science **373**, 352 (2021).

[4] J. Yang, X. Zhu, J. P. F. Nunes, J. K. Yu, R. M. Parrish, T. J. Wolf, M. Centurion, M. Gühr, R. Li, Y. Liu *et al.*, Simultaneous observation of nuclear and electronic dynamics by ultrafast electron diffraction, Science **368**, 885 (2020).

[5] M. Mo, Z. Chen, R. Li, M. Dunning, B. Witte, J. Baldwin, L. Fletcher, J. Kim, A. Ng, R. Redmer *et al.*, Heterogeneous to homogeneous melting transition visualized

with ultrafast electron diffraction, Science **360**, 1451 (2018).

[6] J. Yang, X. Zhu, T. J. Wolf, Z. Li, J. P. F. Nunes, R. Coffee, J. P. Cryan, M. Gühr, K. Hegazy, T. F. Heinz *et al.*, Imaging CF3I conical intersection and photodissociation dynamics with ultrafast electron diffraction, Science **361**, 64 (2018).

[7] S. Duan, Y. Cheng, W. Xia, Y. Yang, C. Xu, F. Qi, C. Huang, T. Tang, Y. Guo, W. Luo, D. Qian, D. Xiang, J. Zhang, and W. Zhang, Optical manipulation of electronic dimensionality in a quantum material, Nature (London) **595**, 239 (2021).

[8] E. J. Sie, C. M. Nyby, C. Pemmaraju, S. J. Park, X. Shen, J. Yang, M. C. Hoffmann, B. Ofori-Okai, R. Li, A. H. Reid *et al.*, An ultrafast symmetry switch in a Weyl semimetal, Nature (London) **565**, 61 (2019).

[9] P. Zhu, Y. Zhu, Y. Hidaka, L. Wu, J. Cao, H. Berger, J. Geck, R. Kraus, S. Pjerov, Y. Shen *et al.*, Femtosecond time-resolved MeV electron diffraction, New J. Phys. **17**, 063004 (2015).

[10] X. Wang, D. Xiang, T. Kim, and H. Ihee, Potential of femtosecond electron diffraction using near-relativistic electrons from a photocathode RF electron gun, J. Korean Phys. Soc. **48**, 583 (2006), https://www.jkps.or.kr/journal/view.html?uid=7476&vmd=Full.

[11] D. H. Dowell and J. F. Schmerge, Quantum efficiency and thermal emittance of metal photocathodes, Phys. Rev. ST Accel. Beams **12**, 074201 (2009).

[12] M. Kozák, N. Schönenberger, and P. Hommelhoff, Ponderomotive generation and detection of attosecond free-electron pulse trains, Phys. Rev. Lett. **120**, 103203 (2018).

[13] M. Kozák, T. Eckstein, N. Schönenberger, and P. Hommelhoff, Inelastic ponderomotive scattering of electrons at a high-intensity optical travelling wave in vacuum, Nat. Phys. **14**, 121 (2018).

[14] J. Lim, Y. Chong, and L. J. Wong, Terahertz-optical intensity grating for creating high-charge, attosecond electron bunches, New J. Phys. **21**, 033020 (2019).

[15] J. Maxson, D. Cesar, G. Calmasini, A. Ody, P. Musumeci, and D. Alesini, Direct measurement of sub-10 fs relativistic electron beams with ultralow emittance, Phys. Rev. Lett. **118**, 154802 (2017).

[16] L. Zhao, J. Wu, Z. Wang, H. Tang, X. Zou, T. Jiang, P. Zhu, D. Xiang, and J. Zhang, Noninvasive time-sorting in radio frequency-compressed ultrafast electron diffraction, Struct. Dyn. **8**, 044303 (2021).

[17] T. Van Oudheusden, P. Pasmans, S. Van Der Geer, M. De Loos, M. Van Der Wiel, and O. Luiten, Compression of subrelativistic space-charge-dominated electron bunches for single-shot femtosecond electron diffraction, Phys. Rev. Lett. **105**, 264801 (2010).

[18] F. Qi, Z. Ma, L. Zhao, Y. Cheng, W. Jiang, C. Lu, T. Jiang, D. Qian, Z. Wang, W. Zhang *et al.*, Breaking 50 femtosecond resolution barrier in MeV ultrafast electron diffraction with a double bend achromat compressor, Phys. Rev. Lett. **124**, 134803 (2020).

[19] H. W. Kim, N. A. Vinokurov, I. H. Baek, K. Y. Oang, M. H. Kim, Y. C. Kim, K.-H. Jang, K. Lee, S. H. Park, S. Park *et al.*, Towards jitter-free ultrafast electron diffraction technology, Nat. Photonics **14**, 245 (2020).

[20] C. Lu, T. Jiang, S. Liu, R. Wang, L. Zhao, P. Zhu, D. Xiang, and J. Zhang, Coulomb-driven relativistic electron beam compression, Phys. Rev. Lett. **120**, 044801 (2018).

[21] L. Zhao, T. Jiang, C. Lu, R. Wang, Z. Wang, P. Zhu, Y. Shi, W. Song, X. Zhu, C. Jing *et al.*, Few-femtosecond electron beam with terahertz-frequency wakefield-driven compression, Phys. Rev. Accel. Beams **21**, 082801 (2018).

[22] E. Snively, M. Othman, M. Kozina, B. Ofori-Okai, S. Weathersby, S. Park, X. Shen, X. Wang, M. Hoffmann, R. Li *et al.*, Femtosecond compression dynamics and timing jitter suppression in a THz-driven electron bunch compressor, Phys. Rev. Lett. **124**, 054801 (2020).

[23] L. Zhao, H. Tang, C. Lu, T. Jiang, P. Zhu, L. Hu, W. Song, H. Wang, J. Qiu, C. Jing *et al.*, Femtosecond relativistic electron beam with reduced timing jitter from THz driven beam compression, Phys. Rev. Lett. **124**, 054802 (2020).

[24] Y. Song, C.-Y. Tsai, K. Fan, J. Yang, and H. Qi, MeV electron bunch compression and timing jitter suppression using a THz-driven resonator, Nucl. Instrum. Methods Phys. Res., Sect. A **1047**, 167774 (2023).

[25] B. Zeitler, K. Floettmann, and F. Grüner, Linearization of the longitudinal phase space without higher harmonic field, Phys. Rev. ST Accel. Beams **18**, 120102 (2015).

[26] C. Li, W. Wang, H. Zhang, Z. Guo, S. Jiang, Z. He, S. Zhang, Q. Jia, L. Wang, and D. He, Relativistic attosecond electron pulses from a photocathode radio-frequency gun, Phys. Rev. Appl. **16**, 054007 (2021).

[27] C. Li, W. Wang, H. Zhang, Z. Guo, X. Xu, Z. He, S. Zhang, Q. Jia, L. Wang, and D. He, Few-femtosecond MeV electron bunches for ultrafast electron diffraction, Phys. Rev. Appl. **17**, 064012 (2022).

[28] H. Yong, S. Sun, B. Gu, and S. Mukamel, Attosecond charge migration in molecules imaged by combined x-ray and electron diffraction, J. Am. Chem. Soc. **144**, 20710 (2022).

[29] H. Yong, D. Keefer, and S. Mukamel, Imaging purely nuclear quantum dynamics in molecules by combined x-ray and electron diffraction, J. Am. Chem. Soc. **144**, 7796 (2022).

[30] M. De Loos and S. Van Der Geer, in *Proceedings of the 5th European Particle Accelerator Conference, EPAC-96, Sitges, Barcelona, Spain* (IOP, Bristol, 1996), p. 1241.

[31] S. Weathersby, G. Brown, M. Centurion, T. Chase, R. Coffee, J. Corbett, J. Eichner, J. Frisch, A. Fry, M. Gühr *et al.*, Mega-electron-volt ultrafast electron diffraction at SLAC National Accelerator Laboratory, Rev. Sci. Instrum. **86**, 073702 (2015).

[32] C. Limborg-Deprey, C. Adolphsen, D. McCormick, M. Dunning, K. Jobe, H. Li, T. Raubenheimer, A. Vrielink, T. Vecchione, F. Wang, and S. Weathersby, Performance of a first generation X-band photoelectron rf gun, Phys. Rev. Accel. Beams **19**, 053401 (2016).

[33] R. A. Marsh, G. G. Anderson, S. G. Anderson, D. J. Gibson, C. P. J. Barty, and Y. Hwang, Performance of a second generation *X*-band rf photoinjector, Phys. Rev. Accel. Beams **21**, 073401 (2018).

[34] B. Spataro, A. Valloni, D. Alesini, N. Biancacci, L. Faillace, L. Ficcadenti, A. Fukusawa, L. Lancia, M. Migliorati, F. Morelli *et al.*, RF properties of a X-band hybrid photoinjector, Nucl. Instrum. Methods Phys. Res., Sect. A **657**, 99 (2011).

[35] D. González-Iglesias, A. Aksoy, D. Esperante, B. Gimeno, A. Latina, M. Boronat, C. Blanch, N. Fuster-Martínez, P. Martinez-Reviriego, P. Martín-Luna *et al.*, X-band RF photoinjector design for the CompactLight project, Nucl. Instrum. Methods Phys. Res., Sect. A **1014**, 165709 (2021).

[36] W. Tan, S. Antipov, D. Doran, G. Ha, C. Jing, E. Knight, S. Kuzikov, W. Liu, X. Lu, P. Piot *et al.*, Demonstration of sub-GV/m accelerating field in a photoemission electron gun powered by nanosecond X-band radio-frequency pulses, Phys. Rev. Accel. Beams **25**, 083402 (2022).

[37] Y. I. Salamin, Electron acceleration from rest in vacuum by an axicon Gaussian laser beam, Phys. Rev. A **73**, 043402 (2006).

[38] R. Li, P. Musumeci, H. Bender, N. Wilcox, and M. Wu, Imaging single electrons to enable the generation of ultrashort beams for single-shot femtosecond relativistic electron diffraction, J. Appl. Phys. **110**, 074512 (2011).